Spectral function and excited states in lattice QCD with the maximum entropy method

T. Yamazaki,[1] S. Aoki,[1] R. Burkhalter,[1,2] M. Fukugita,[3] S. Hashimoto,[4] N. Ishizuka,[1,2] Y. Iwasaki,[1,2] K. Kanaya,[1] T. Kaneko,[4] Y. Kuramashi,[4] M. Okawa,[4] Y. Taniguchi,[1] A. Ukawa,[1,2] and T. Yoshié[1,2]

(CP-PACS Collaboration)

[1]*Institute of Physics, University of Tsukuba, Tsukuba, Ibaraki 305-8571, Japan*
[2]*Center for Computational Physics, University of Tsukuba, Tsukuba, Ibaraki 305-8577, Japan*
[3]*Institute for Cosmic Ray Research, University of Tokyo, Kashiwa, Chiba 277-8582, Japan*
[4]*High Energy Accelerator Research Organization (KEK), Tsukuba, Ibaraki 305-0801, Japan*

(Received 30 May 2001; published 20 November 2001)

We apply the maximum entropy method to extract the spectral functions for pseudoscalar and vector mesons from hadron correlators previously calculated at four different lattice spacings in quenched QCD with the Wilson quark action. We determine masses and decay constants for the ground and excited states of the pseudoscalar and vector channels from the position and area of peaks in the spectral functions. We obtain the results $m_{\pi_1}=660(590)$ MeV and $m_{\rho_1}=1540(570)$ MeV for the first excited state masses, in the continuum limit of quenched QCD. We also find unphysical states that have an infinite mass in the continuum limit, and argue that they are bound states of two doublers of the Wilson quark action. If the interpretation is correct, this is the first time that the state of doublers has been identified in lattice QCD numerical simulations.

DOI: 10.1103/PhysRevD.65.014501 PACS number(s): 11.15.Ha, 12.38.Gc

I. INTRODUCTION

The spectral function of hadron correlation functions contains information not only on the mass of the ground state but also on other quantities such as the masses for excited states, and decays and scatterings of hadrons. In lattice QCD simulations one can numerically obtain a Euclidean time correlation function $D(\tau)$ of an operator $O(\tau)$, which is related to the spectral function $f(\omega)$ of this correlator through

$$D(\tau)=\langle 0|O(\tau)O^{\dagger}(0)|0\rangle = \int d\omega f(\omega)K(\omega,\tau), \quad (1)$$

where $K(\tau,\omega)$ is a kernel of the Laplace transformation given by

$$K(\omega,\tau)=e^{-\omega\tau}+e^{-\omega(T-\tau)}$$

for $0\leqslant\tau\leqslant T$ with the periodic boundary condition, where T is the lattice size in the Euclidean time direction. A typical form of $f(\omega)$ is

$$f(\omega)=Z_0\delta(\omega-E_0)+\tilde{f}(\omega;\omega\geqslant 2m_0), \quad (2)$$

where E_0 is the energy of the ground state $|E_0\rangle$ coupled to the operator O and $Z_0=|\langle 0|O|E_0\rangle|^2$, and $\tilde{f}(\omega)$ represents the continuous spectrum which starts at $\omega=2m_0$ for the two-particle state.

In principle one can extract all the information for the states that can couple to the operator O from the spectral function $f(\omega)$. In the usual analysis of lattice QCD simulations, however, only the mass (or energy) of the ground state E_0 and its amplitude Z_0 can be reliably extracted from the asymptotic behavior of the point source correlation function at large Euclidean times,

$$D(\tau)\to Z_0e^{-E_0\tau}, \quad \tau\to\infty.$$

Numerically, the extraction of masses of excited states with a multiexponential fit to a single correlation function is unstable, so that a simultaneous fit to several correlation functions that have the same set of intermediate states with different amplitudes becomes necessary to stabilize the result. Different operators that have larger overlaps with the excited state may also be employed to extract the mass of the excited state. Similar but more difficult problems appear in the calculation of the decay amplitude [1,2].

If one could reconstruct $f(\omega)$ directly from the correlation function $D(\tau)$ using data at all τ, information of various states could be extracted from one correlation function. It is simple and efficient, since one can avoid more complicated procedures needed in the usual extraction, such as the tuning of operators, the calculation of several correlation functions, etc. Since the number of data for $D(\tau)$ with a discrete set of time τ is much smaller than the number of degrees of freedom necessary for the reconstruction of $f(\omega)$ in general, however, the standard χ^2 fit is ill posed for this problem. With some assumptions about the form of the spectral function the χ^2 fit may work, but this is essentially equivalent to the multiexponential or more complicated fit to the correlation function.

In condensed matter physics, the reconstruction of the spectral function in quantum Monte Carlo simulations has been attempted with the maximum entropy method (MEM) [3]. It has also been successfully applied for image reconstruction in astrophysics. The most important assumption in the MEM is that a probability for spectral functions can be assigned for given data of $D(\tau)$. Then the MEM can numerically reconstruct the most probable spectral function, using Bayes's theorem in probability theory, without any strong constraints on its form. Recently, this method has been tested in lattice QCD [4,5] and the first interesting results for the

spectral function have been obtained [6–8].

In this paper, we employ the MEM to reconstruct the spectral functions of pseudoscalar and vector mesons from the correlation functions previously calculated on lattices with the spatial size about 3 fm at four different lattice spacings in quenched QCD [9,10]. From the spectral functions we extract masses and decay constants for excited states as well as for the ground state. While they agree with results obtained from the exponential fits to the correlation functions, the errors for the excited state masses from the spectral function are smaller than those from the multiexponential fit, so that we can estimate masses for excited states in the continuum limit with reasonable errors. We also find evidence that some excited states are composed of fermion doublers.

This paper is organized as follows. In Sec. II, we summarize our implementation of the MEM and present results from tests using mock-up data generated from a realistic spectral function. Some details of the lattice QCD data and parameters used in our MEM analysis are given in Sec. III. In Sec. IV, we present our results for the spectral function, which show excited state peaks as well as the ground state peak. From the positions and the areas of these peaks we extract masses and decay constants, and compare them with those obtained directly from correlation functions. The continuum extrapolation is made for these quantities. In Sec. V, we argue that some peaks in the spectral functions correspond to a state containing two doublers of the Wilson quarks. Our conclusions are given in Sec VI. In the Appendixes technical details of the MEM are collected.

II. MAXIMUM ENTROPY METHOD

A. Implementation

The existence of a probability distribution for a spectral function is a key assumption in the maximum entropy method. Using this assumption one can obtain the most probable spectral function for given lattice data D and all prior knowledge H, such as $f(\omega)\geqslant 0$, by maximizing the conditional probability $\mathrm{P}[F|DH]$, where $\mathrm{P}[F|DH]$ is the probability of F with the condition that D and H are given. Here F stands for the spectral function $f(\omega)$. Using Bayes's theorem in probability theory [11],

$$\mathrm{P}[X|YZ]=\frac{\mathrm{P}[Y|XZ]\,\mathrm{P}[X|Z]}{\mathrm{P}[Y|Z]}, \tag{3}$$

where $\mathrm{P}[X]$ is the probability of an event X, one rewrites the conditional probability $\mathrm{P}[F|DH]$ as

$$\mathrm{P}[F|DH]\propto \mathrm{P}[D|FH]\,\mathrm{P}[F|H]. \tag{4}$$

Here $\mathrm{P}[D|FH]$ is the probability of data for a given spectral function, called the likelihood function, and $\mathrm{P}[F|H]$ is the probability of the spectral function for given prior knowledge, called the prior probability.

The likelihood function is equivalent to χ^2 in the least squares method [12]. For a large number of Monte Carlo measurements of a correlation function, the data are expected to obey a Gaussian distribution according to the central limit theorem, which gives

$$\mathrm{P}[D|FH]=\frac{1}{Z_L}e^{-L}, \tag{5}$$

$$L=\frac{1}{2}\sum_{i,j}^{N_D}[D(\tau_i)-D_f(\tau_i)]C_{ij}^{-1}[D(\tau_j)-D_f(\tau_j)], \tag{6}$$

with the normalization constant $Z_L=(2\pi)^{N_D}\sqrt{\det C}$, and the number of temporal points N_D. The lattice propagator data averaged over gauge configurations, $D(\tau)$, and the covariance matrix C are defined by

$$D(\tau_i)=\frac{1}{N_{conf}}\sum_{n=1}^{N_{conf}}D^n(\tau_i), \tag{7}$$

$$C_{ij}=\frac{1}{N_{conf}(N_{conf}-1)}\sum_{n=1}^{N_{conf}}[D(\tau_i)-D^n(\tau_i)]\times[D(\tau_j)-D^n(\tau_j)], \tag{8}$$

where N_{conf} is the total number of gauge configurations and $D^n(\tau)$ are the data for the nth gauge configuration. Finally, $D_f(\tau)$ is the propagator constructed from the spectral function $f(\omega)$ and the kernel $K(\omega,\tau)$ as

$$D_f(\tau)=\int d\omega f(\omega)K(\omega,\tau). \tag{9}$$

The prior probability is written in terms of the entropy $S(f)$ [13–16] for a given model $m(\omega)$ represented by a real and positive function, and a real and positive parameter α. The entropy $S(f)$ becomes zero at its maximum point where $f(\omega)$ is equal to $m(\omega)$. Explicitly, we have

$$\mathrm{P}[F|Hm\alpha]=\frac{1}{Z_S(\alpha)}e^{\alpha S}, \tag{10}$$

$$S(f)=\int d\omega\left[f(\omega)-m(\omega)-f(\omega)\log\left(\frac{f(\omega)}{m(\omega)}\right)\right] \tag{11}$$

$$\rightarrow\sum_{l=1}^{N_\omega}\left[f_l-m_l-f_l\log\left(\frac{f_l}{m_l}\right)\right], \tag{12}$$

with the normalization constant $Z_S(\alpha)=(2\pi/\alpha)^{N_\omega/2}$ calculated in Appendix C. In Eq. (12) the continuous spectral function $f(\omega)$ is approximately represented by a discrete set of points $f(\omega_l)=f_l$ with $l=1,\ldots,N_\omega$. Hereafter we replace the prior knowledge H in Eq. (4) by $Hm\alpha$, writing m and α explicitly. It is worth mentioning that this form of the entropy leads to a positive spectral function in the MEM.

Combining Eqs. (5) and (10), one obtains

$$\mathrm{P}[F|DHm\alpha] \propto \frac{e^{Q_\alpha(f)}}{Z_L Z_S(\alpha)}, \quad Q_\alpha(f) = \alpha S(f) - L. \quad (13)$$

Therefore the condition satisfied by the most probable spectral function f_α for a given α [and model $m(\omega)$] is given by

$$\left.\frac{\delta Q_\alpha(f)}{\delta f}\right|_{f=f_\alpha} = 0. \quad (14)$$

The parameter α dictates the relative weight of the entropy $S(f)$ and L. One can deal with α dependence of f_α as follows. One first defines $\mathrm{P}[\alpha|DHm]$ [3,13,14], the probability of α for given data and all prior knowledge, which can be transformed as

$$\mathrm{P}[\alpha|DHm] \propto \mathrm{P}[\alpha|Hm] \int \mathcal{D}F \frac{e^{Q_\alpha(f)}}{Z_L Z_S(\alpha)}. \quad (15)$$

See Appendix E for details. In the final result $\hat{f}(\omega)$, α is averaged with this weight factor $\mathrm{P}[\alpha|DHm]$,

$$\hat{f}(\omega) = \int d\alpha \mathrm{P}[\alpha|DHm] f_\alpha(\omega) \Big/ \int d\alpha\, \mathrm{P}[\alpha|DHm]. \quad (16)$$

This procedure is called Bryan's method [17] and is used in this article. We restrict the range of α in the actual average as $\alpha_{min} \leqslant \alpha \leqslant \alpha_{max}$, where α_{min} and α_{max} are chosen to satisfy $\mathrm{P}[\hat{\alpha}|DHm] \geqslant 10\,\mathrm{P}[\alpha_{min,max}|DHm]$ with $\hat{\alpha}$ being the maximum value of $\mathrm{P}[\alpha|DHm]$. The standard choice of $\mathrm{P}[\alpha|Hm]$ in Eq. (15) is either a constant or $1/\alpha$ [3,14,17]. In the next section we will show that the final result is insensitive to the choice as long as $\mathrm{P}[\alpha|DHm]$ is sharply peaked around $\hat{\alpha}$, and therefore we adopt $\mathrm{P}[\alpha|Hm] = \mathrm{const}$ in our main analysis.

In the MEM it is not possible to assign error bars to each point in the spectral function since the errors between different points are strongly correlated. Instead we estimate the uncertainty of the spectral function averaged over ω in a certain region by the method explained in Appendix F. The magnitude of this uncertainty gives an estimate for the goodness of the given model $m(\omega)$ [3,6].

B. Test

Several tests of the MEM have already been carried out in Ref. [6], where the dependence of the results on the number of time slices N_D, the size of errors of the data, and the model $m(\omega)$ have been examined using mock-up data created from test spectral functions. The following conclusions were drawn from the tests.

(1)Decreasing the error of data $D(\tau)$ is more important than increasing N_D for obtaining better estimates of $f(\omega)$ that reproduce the original spectral function more closely.

(2) It is better to include information about $f(\omega)$, such as the asymptotic value, if it is known, into the model $m(\omega)$.

(3) If the obtained $f(\omega)$ depends strongly on the model, a better model in the sense of leading to an $f(\omega)$ that is closer to the original spectral function gives smaller errors for the averaged $f(\omega)$.

(4) The error of the averaged $f(\omega)$ in a certain region can be used to measure the significance of $f(\omega)$ in the region. For example, if the error of the averaged $f(\omega)$ around a peak is much smaller than the averaged value, the peak is likely to be true, and vice versa.

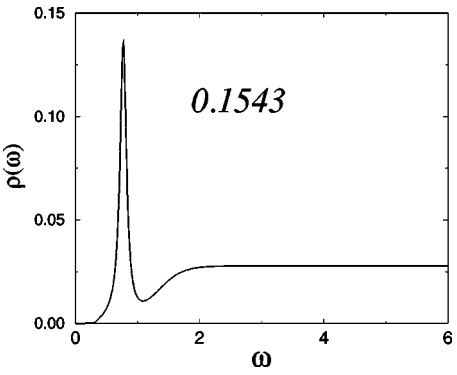

FIG. 1. The input spectral function $\rho_{in}(\omega)$. The value in the figure is the area under the curve for $0 \leqslant \omega \leqslant 6$.

Before applying the MEM to actual data, we perform further tests on (a) the dependence on N_D and the temporal separation of data $\Delta\tau$, and (b) the dependence on the choice of $\mathrm{P}[\alpha|Hm]$. For these tests we use a realistic spectral function in the vector channel of the e^+e^- annihilation [6,18], which is given by $f_{in}(\omega) = \rho_{in}(\omega)\omega^2$, where the factor ω^2 is expected from the dimension of meson spectral function, with

$$\rho_{in}(\omega) = \frac{2}{\pi}\left[F_\rho^2 \frac{\Gamma_\rho(\omega) m_\rho}{(\omega^2 - m_\rho^2)^2 + \Gamma_\rho^2(\omega) m_\rho^2} + \frac{1}{8\pi}\left(1 + \frac{\alpha_s}{\pi}\right)\frac{1}{1 + e^{(\omega_0 - \omega)/\delta}}\right]. \quad (17)$$

Here F_ρ is the residue of ρ meson resonance defined by

$$\langle 0|\bar{d}\gamma_\mu u|\rho\rangle = \sqrt{2} F_\rho m_\rho \epsilon_\mu = \sqrt{2} f_\rho m_\rho^2 \epsilon_\mu, \quad (18)$$

with the polarization vector ϵ_μ, and $\Gamma_\rho(\omega)$ includes the θ function which represents the threshold of $\rho \to \pi\pi$ decay as

$$\Gamma_\rho(\omega) = \frac{1}{48\pi}\frac{m_\rho^3}{F_\rho^2}\left(1 - \frac{4m_\pi^2}{\omega^2}\right)^{3/2} \theta(\omega - 2m_\pi). \quad (19)$$

We make dimensionful quantities dimensionless using the lattice spacing a, $\omega \to \omega a$, $\tau \to \tau/a$ where a is set to 1 GeV^{-1}. The values of parameters are

$$m_\rho = 0.77, \quad m_\pi = 0.14, \quad F_\rho = 0.142,$$
$$\omega_0 = 1.3, \quad \delta = 0.2, \quad \alpha_s = 0.3, \quad (20)$$

where α_s is independent of ω for simplicity. The shape of $\rho_{in}(\omega)$ for this choice of parameters is shown in Fig. 1. The

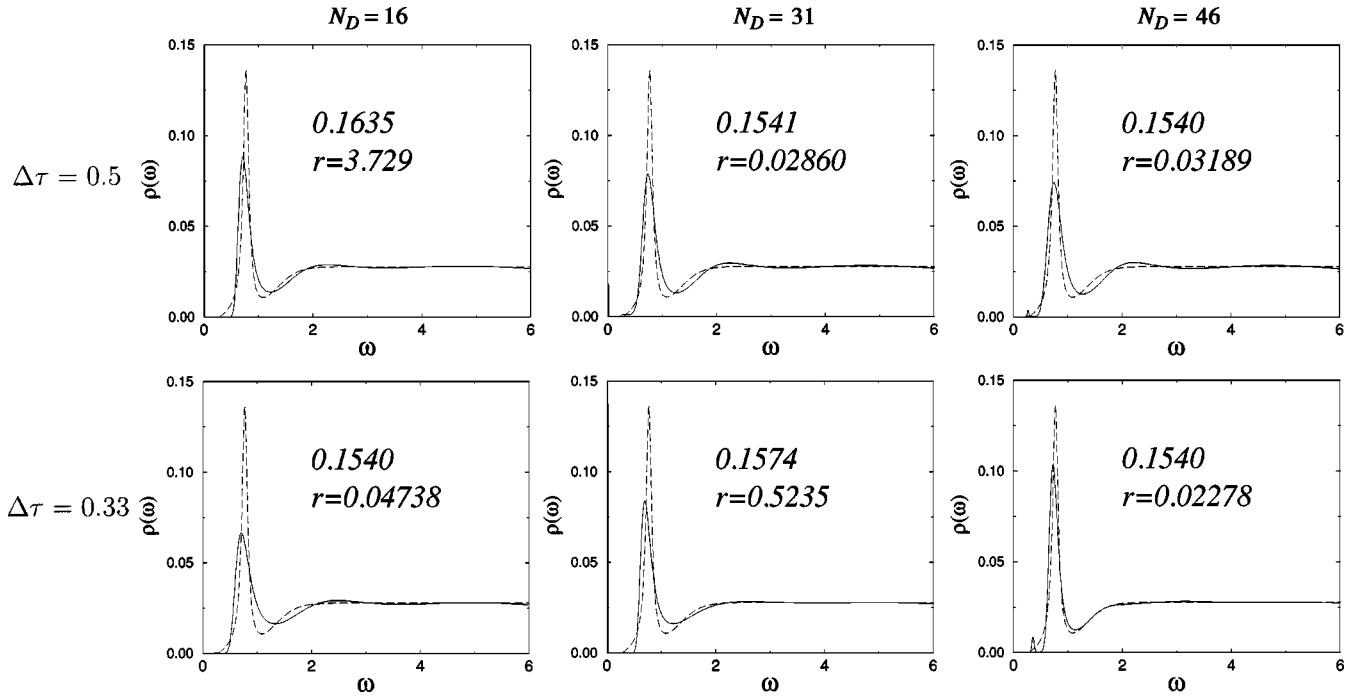

FIG. 2. The output spectral function $\rho_{out}(\omega)$ obtained by the MEM for different $\Delta\tau$ and N_D is shown by solid lines. The input $\rho_{in}(\omega)$ is shown by long dashed lines. The values in each figure are the area of $\rho_{out}(\omega)$ and $r=\Sigma_{l=1}^{N_\omega}[\rho_{in}(\omega_l)-\rho_{out}(\omega_l)]^2$.

value in the figure represents the area of $\rho_{in}(\omega)$ for $0\leqslant\omega\leqslant 6$.

We make mock-up data $D(\tau)$ from $f_{in}(\omega)$ as follows. (i) The central value of $D(\tau)$ is given by integrating the spectral function $f_{in}(\omega)$ and a kernel $K(\omega,\tau)=e^{-\omega\tau}$ over ω in the same way as for $D_f(\tau)$ in Eq. (6). (ii) Errors of $D(\tau)$ are generated by Gaussian random numbers with the variance $\sigma(\tau_i)=be^{a\tau_i}D(\tau_i)$, $a=0.1$, $b=10^{-10}$, in order to incorporate the fact that the error of lattice correlation functions increases as τ increases.

In this test, no correlation between different τ is taken into account; thus the covariance matrix C is set to be diagonal. The model function is given by $m(\omega)=m_0\omega^2$ with $m_0=0.0277$, which is motivated by the value of $\rho_{in}(\omega\rightarrow\infty)$. We set the maximum value of ω, $\omega_{max}=6$, the ω space is discretized with an equal separation $\Delta\omega=0.01$, and $N_\omega=600$. We also calculate the area of the MEM result $\rho_{out}(\omega)$ for $0\leqslant\omega\leqslant\omega_{max}$ and define $r=\Sigma_{l=1}^{N_\omega}[\rho_{in}(\omega_l)-\rho_{out}(\omega_l)]^2$, to measure the difference between ρ_{in} and ρ_{out}.

We summarize the results for $\rho_{out}(\omega)$ in various cases as follows.

(a) To investigate the dependence of $\rho_{out}(\omega)$ on $\Delta\tau$ and N_D, we extract $\rho_{out}(\omega)$ by the MEM, from data with $\Delta\tau=0.5$,0.33 and $N_D=16$,31,46, as shown in Fig. 2. Data at large τ are necessary to reconstruct $\rho_{out}(\omega)$ at small ω correctly, as seen from the fact that a false peak sometimes appears around $\omega=0$ from data with $\Delta\tau=0.5$ and $N_D=16$ $[\tau_{max}=\Delta\tau(N_D-1)=7.5]$ or with $\Delta\tau=0.33$ and $N_D=31$ $(\tau_{max}=10)$. Once τ_{max} becomes large enough (larger than 15 in this case), a smaller $\Delta\tau$ is better for the result, as seen from the comparison between results from data with $\Delta\tau=0.5$ and $\Delta\tau=0.33$ at $N_D=46$.

(b) We also check the dependence of $\rho_{out}(\omega)$ on two forms of $\mathrm{P}[\alpha|Hm]$, $\mathrm{P}[\alpha|Hm]=$constant or $1/\alpha$. As shown in Fig. 3, the two choices give almost identical shapes of $\rho_{out}(\omega)$, although the weight factor $\mathrm{P}[\alpha|DHm]$ is rather different between the two cases.

Our investigations add further information on the parameter dependence of the result in the MEM, which we summarize as the following three points.

(5) $\tau_{max}=\Delta\tau(N_D-1)$ must be sufficiently large for a reliable result of $f(\omega)$.

(6) Once τ_{max} is taken large enough, a smaller $\Delta\tau$ is better.

(7) The result $\rho_{out}(\omega)$ is insensitive to the choice of $\mathrm{P}[\alpha|Hm]$.

III. LATTICE QCD DATA AND PARAMETERS IN MEM ANALYSIS

We now apply the MEM to the lattice correlation functions previously obtained in quenched QCD [9,10] with the plaquette action for gluons and the Wilson action for quarks. The simulation was performed at four values of β, corresponding to $a^{-1}=2$–4 GeV for the continuum extrapolation, on $32^3\times 56$ to $64^3\times 112$ lattices with spatial size about 3 fm. The simulation parameters are compiled in Table I. At each β, five values of the hopping parameter κ, which correspond to $m_\pi/m_\rho\approx$ 0.75, 0.7, 0.6, 0.5, and 0.4, were employed for the chiral extrapolation. The values of the hopping parameters are numbered from heavy to light in Table I. For example, we call the κ corresponding to the lightest and heaviest quark masses $K51$. Except for an additive renormal-

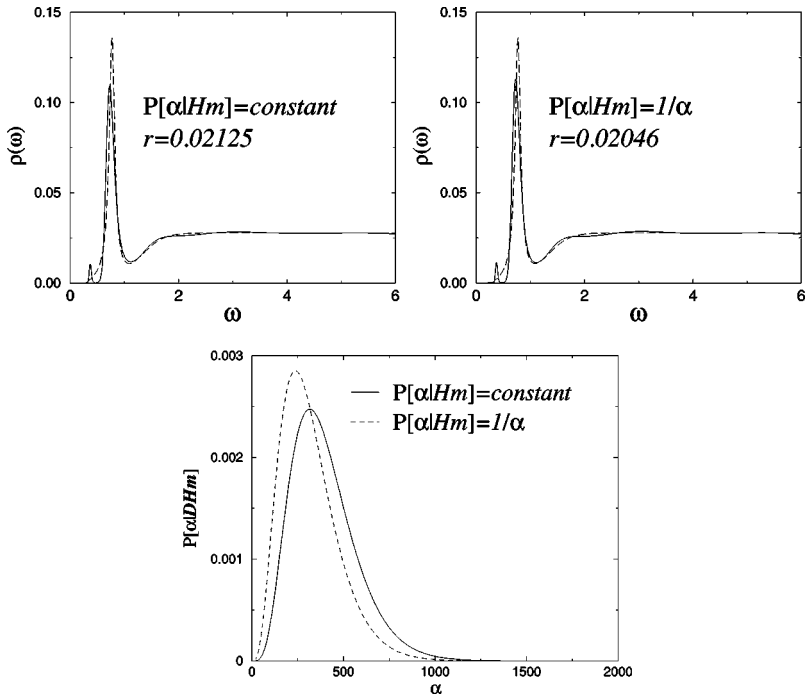

FIG. 3. Influence of the choice of $P[\alpha|Hm]$. The left figure is for $P[\alpha|Hm]=\text{const}$ and the right for $P[\alpha|Hm]=1/\alpha$. The figure below shows the corresponding $P[\alpha|DHm]$ normalized to unity for which data with $\Delta\tau=0.33$ and $N_D=46$ are used. The input $\rho_{in}(\omega)$ is shown by the long dashed lines, and $r=\Sigma_{l=1}^{N_\omega}[\rho_{in}(\omega_l)-\rho_{out}(\omega_l)]^2$ represents the difference from $\rho_{in}(\omega)$.

ization factor, the average quark mass is equal to the average inverse hopping parameter K^{-1} given by

$$K^{-1}=\frac{1}{2}(\kappa_1^{-1}+\kappa_2^{-1}), \tag{21}$$

where κ_1 and κ_2 are the hopping parameters of the quark and antiquark in the meson.

In our MEM analysis, we employ pseudoscalar and vector meson correlation functions, defined by

$$\sum_{\mathbf{x}}\langle\bar{d}\Gamma u(\tau,\mathbf{x})(\bar{d}\Gamma u)^{\dagger}(0,\mathbf{0})\rangle=\int d\omega f(\omega)K(\omega,\tau), \tag{22}$$

where Γ is γ_5 (γ_μ) for the pseudoscalar (vector) meson, $f(\omega)$ is a spectral function, and $K(\omega,\tau)$ is a kernel. We use only point source data to satisfy the condition that $f(\omega)\geqslant 0$. Since the spectral function of the meson propagator has dimension 2, we define a dimensionless function $\rho(\omega)$ as

$$f(\omega)=\rho(\omega)\omega^2. \tag{23}$$

The model is chosen to be $m(\omega)=m_0\omega^2$ and the value of m_0 is taken equal to the asymptotic value of $\rho(\omega)$ in perturbation theory [6] given by

$$m_0=\frac{C_1}{4\pi^2}\left(1+C_2\frac{\alpha_s}{\pi}\right)\left(\frac{1}{Z^2}\prod_{i=1}^{2}\frac{1}{2\kappa_i}\right), \tag{24}$$

TABLE I. Simulation parameters of hadron propagator data [9,10] used in the present MEM analysis. The numbering of hopping parameters is introduced for convenience. The smallest number corresponds to the heaviest quark mass, and vice versa.

β	Lattice size(L^3T)	Conf. #	Sweep/Conf.
5.90	32^3 56	800	200
6.10	40^3 70	600	400
6.25	48^3 84	420	1000
6.47	64^3 112	150	2000

	Hopping parameter κ				
β	1	2	3	4	5
5.90	0.1566	0.1574	0.1583	0.1589	0.1592
6.10	0.1528	0.1534	0.1540	0.1544	0.1546
6.25	0.15075	0.15115	0.15165	0.15200	0.15220
6.47	0.14855	0.14885	0.14925	0.14945	0.14960
m_π/m_ρ	0.75	0.7	0.6	0.5	0.4

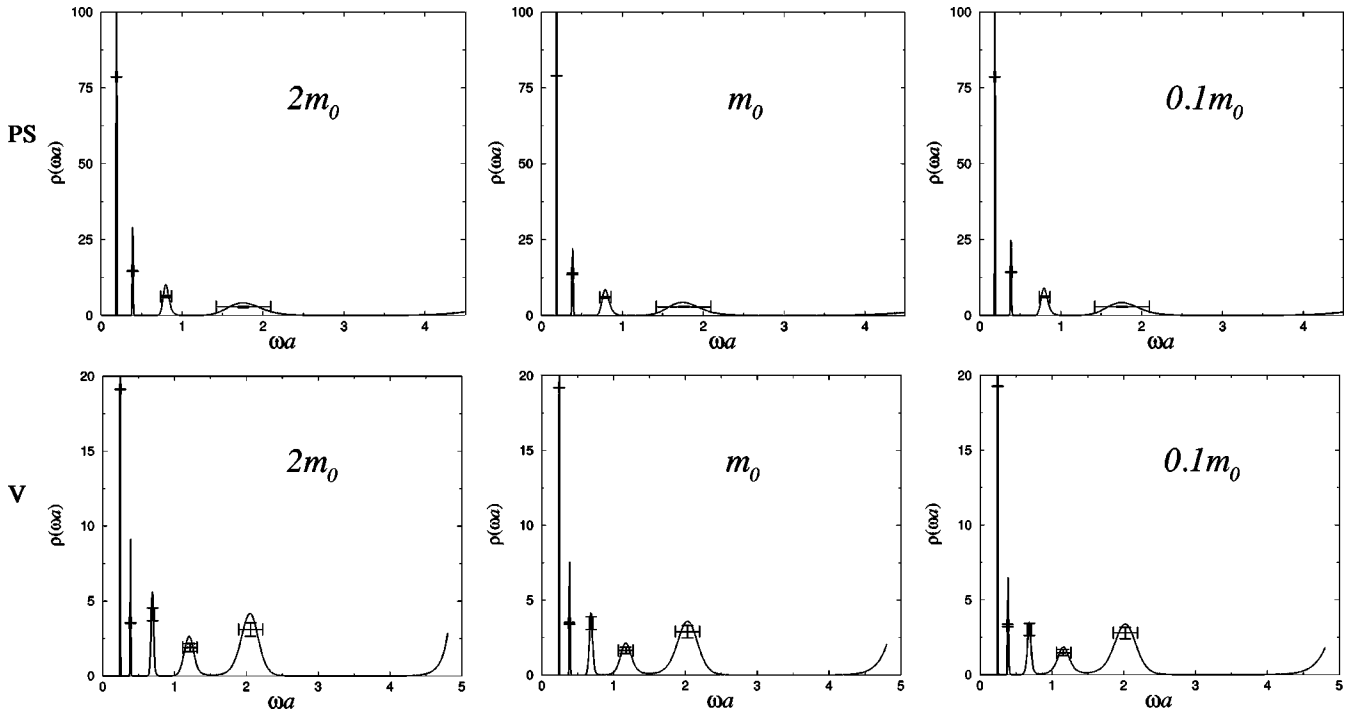

FIG. 4. Model (m_0) dependence for pseudoscalar (PS) and vector (V) channels at $\beta=6.47$ and $K11$.

where α_s is the strong coupling constant, the coefficients C_i are perturbatively calculated in continuum QCD [19], and Z is the renormalization constant for the pseudoscalar (PS) or vector (V) operator. The spectral function from our data is insensitive to the value of m_0, as shown in Fig. 4, where $f(\omega)$ obtained with three different models is plotted for pseudoscalar and vector mesons at $\beta=6.47$ and $K11$. In the figure the horizontal bars indicate the region over which the result is averaged, while the vertical bars indicate the uncertainty in the averaged value of the result. Both the averaged spectral functions and their uncertainties are almost identical for the different models. Because of this property, we simply take $\alpha_s=0.21$ and employ the nonperturbative $Z_{\rm V}$ and the perturbative $Z_{\rm PS}$ calculated at $\beta=5.90$ in Eq. (24) for all β. The normalization factor $1/2\kappa$ is used also for the pseudoscalar meson with tadpole-improved $Z_{\rm PS}$. The values of Z as well as C_i are given in Table II.

Other parameters in the MEM analysis such as N_D and $(\omega a)_{max}$ are determined as follows. We take N_D as large as possible unless the error of the data becomes too large for a reliable result, and we choose $(\omega a)_{max}\geqslant\pi$ and increase it until the result becomes stable. Both parameters are also given in Table II. For $\Delta\omega$, which should be smaller than $1/T$, we take $\Delta\omega=10^{-4}$ around the peak of the ground state to determine the ground state mass accurately, and $\Delta\omega=2.5\times10^{-3}$ away from the peak.

TABLE II. Parameters used in the MEM analysis. The lower part shows $(N_D,(\omega a)_{max})$.

	C_1	C_2	Z	
PS	3/2	11/3	0.728	
V	1	1	0.536	
β	5.90	6.10	6.25	6.47
PS	(20,4.0)	(32,4.5)	(32,4.5)	(45,4.5)
V	(21,4.2)	(30,4.8)	(30,4.8)	(30,4.8)

IV. RESULTS

In this section, we present our results for the spectral functions of pseudoscalar and vector meson propagators, from which we extract physical quantities such as masses and decay constants.

A. Spectral functions

Our results for $\rho(\omega)$ obtained from meson propagators by the MEM for three different K^{-1} at all β are compiled in Fig. 5. The lowest peak corresponds to the ground state, the next peak corresponds to the first excited state, and so on. At fixed β, the positions for these peaks move toward smaller ω as the quark mass decreases. This shows that the meson masses decrease with decreasing quark mass, as expected. The number of peaks increases from $\beta=5.90$ to $\beta=6.47$ for both pseudoscalar and vector channels, since more states with higher energy appear in spectral functions for larger lattice cutoff (smaller lattice spacing). All peak positions move to smaller values as β increases, except the peaks at $\omega a\approx1.7$ for the pseudoscalar channel and at $\omega a\approx2$ for the vector channel. Thus the masses in the physical limits stay finite, except those of the latter peaks which become infinite. We discuss these unphysical states in more detail in the next section.

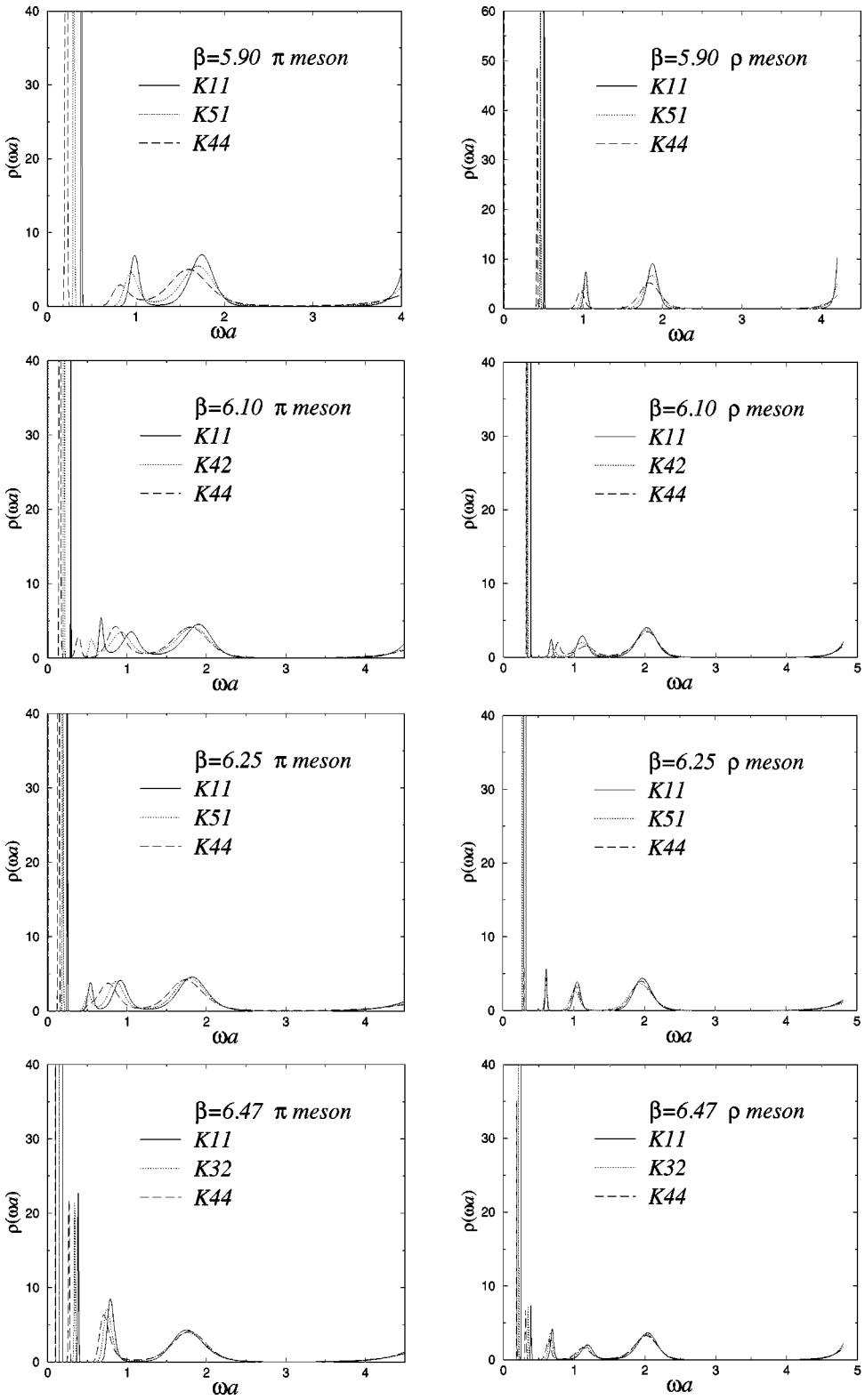

FIG. 5. Spectral functions at all β obtained by the MEM for different values of K^{-1}. On the left hand side the π meson spectral function and on the right hand side the ρ meson spectral function are shown. The state at $\omega a \approx 2$ is considered as unphysical since its position does not move with β.

TABLE III. Comparison of the MEM analysis with the double exponential fit, using the vector meson correlation function at $\beta = 5.90$. The symbol Kn_1n_2 expresses the quark mass used in the correlation function, n_1 and n_2 being defined in Table I. DOF indicates degrees of freedom.

	Exponential fit			MEM	
	Ground	Excited	χ^2/DOF	Ground	Excited
$K11$	0.5093(11)	1.08(11)	0.220	0.5094(16)	1.034(30)
$K22$	0.4784(12)	1.08(14)	0.359	0.4789(20)	1.018(37)
$K31$	0.4772(15)	1.08(14)	0.466	0.4779(20)	1.020(36)
$K32$	0.4613(15)	1.07(15)	0.587	0.4623(23)	1.009(40)
$K33$	0.4435(22)	1.03(19)	0.687	0.4451(27)	0.997(44)
$K41$	0.4668(23)	1.09(17)	0.638	0.4678(23)	1.020(37)
$K42$	0.4505(22)	1.06(22)	0.750	0.4519(27)	1.006(44)
$K44$	0.4214(43)	1.08(21)	0.890	0.4218(43)	0.969(58)
$K51$	0.4622(20)	1.15(21)	0.771	0.4630(25)	1.020(40)
$K52$	0.4460(32)	1.11(19)	0.872	0.4469(30)	1.004(46)
$K55$	0.4107(37)	1.19(20)	1.191	0.4080(65)	0.929(70)

B. Meson masses

From the peak positions of the spectral function, we determine the masses of excited states as well as the ground state. The errors of these masses are estimated by the single elimination jackknife method.

In order to check whether the peaks in the spectral function really correspond to particle states in correlation functions, we also extract the masses of the ground and first excited states by fitting the correlation functions with a double exponential form. In order to obtain the mass of the first excited state reliably, correlation functions from both point and ground state smeared sources for the ρ meson are simultaneously fitted. Results at $\beta = 5.90$ are given in Table III and Fig. 6, where errors are again evaluated with the single elimination jackknife method, together with those obtained by the MEM. We find that the ground state masses from the two methods agree very well, and the first excited state masses are consistent with each other within the statistical error. It is noted that the error of the first excited state obtained by the MEM is smaller than that from the double exponential fit to our data. This does not mean that the error for the first excited state mass obtained by the MEM is always smaller than the one from a multiexponential fit. If one employed more sophisticated methods, such as diagonalization of the matrix of several correlation functions or use of an excited state smeared source, the standard method could give a smaller error for the excited state. The merit of the MEM, however, is that such information can be extracted from a point source correlation function, so that further numerical simulations are unnecessary.

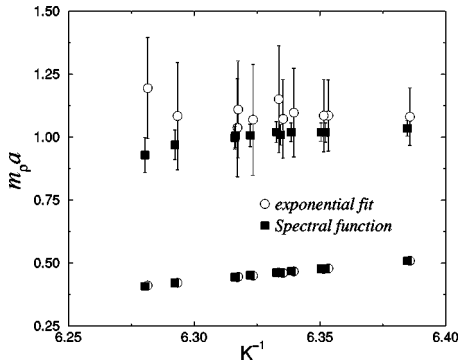

FIG. 6. Comparison of the ρ meson mass for the ground and first excited states from the spectral function and that from the double exponential fit. Circles are slightly shifted to larger K^{-1}.

We determine the chiral limit and the critical hopping parameter κ_c where the ground state of the π meson mass vanishes by extrapolating $(m_\pi a)^2$ linearly in K^{-1}. For other states, including the excited states of π mesons, the masses ma themselves obtained from the spectral function are extrapolated linearly in K^{-1} to the chiral limit. The chiral extrapolation at each β is shown in Fig. 7. Some excited state peaks do not appear in the spectral functions obtained from some jackknife samples. These masses are excluded from the chiral extrapolation and are not plotted in the figures. The lattice spacing a is fixed by setting the ground state mass for the ρ meson in the chiral limit to the experimental value $m_\rho = 770$ MeV. All dimensionful quantities are normalized by the ρ meson mass in the chiral limit.

The masses in the chiral limit are compiled in Table IV, together with the result of the standard analysis [9,10] for the lattice spacing, which agrees with the values from the present MEM analysis. At $\beta = 6.47$, our lattice spacing has a larger error. This is caused by large errors of point source data at this β. As shown in Fig. 8, the ground state masses for each K^{-1} agree with the previous results from the exponential fit of ground state smeared source data [10].

The masses of the excited states in the chiral limit are extrapolated to the continuum limit, except for the unphysical states mentioned before, as shown in Fig. 9. We see that the mass of the first excited state is consistent with the one reported in Ref. [6] for both π and ρ mesons. Note that the error for the first excited state of the ρ meson from the double exponential fit at $\beta = 5.90$ (square) is too large for a reasonable continuum extrapolation. The mass ratios in the continuum limit are given in Table V. The mass of the first excited state normalized by the ground state mass of ρ meson for the π meson in the continuum limit is 0.86(77), which should be compared with the experimental value 1.68(12), while the mass for the ρ meson is 2.00(74) in comparison to the experimental value of 1.90(3) or 2.20(2) (there are two candidates for the first excited state of the ρ meson in experiment). The first excited state masses for both mesons are consistent with experimental values albeit the errors are quite large. For the ρ meson we are not able to decide whether the first excited state is $\rho(1450)$ or $\rho(1700)$ due to the large error of our result.

C. Decay constants

From the spectral function we can also extract the decay constants for the ground states of π and ρ mesons, f_π and f_ρ, defined by

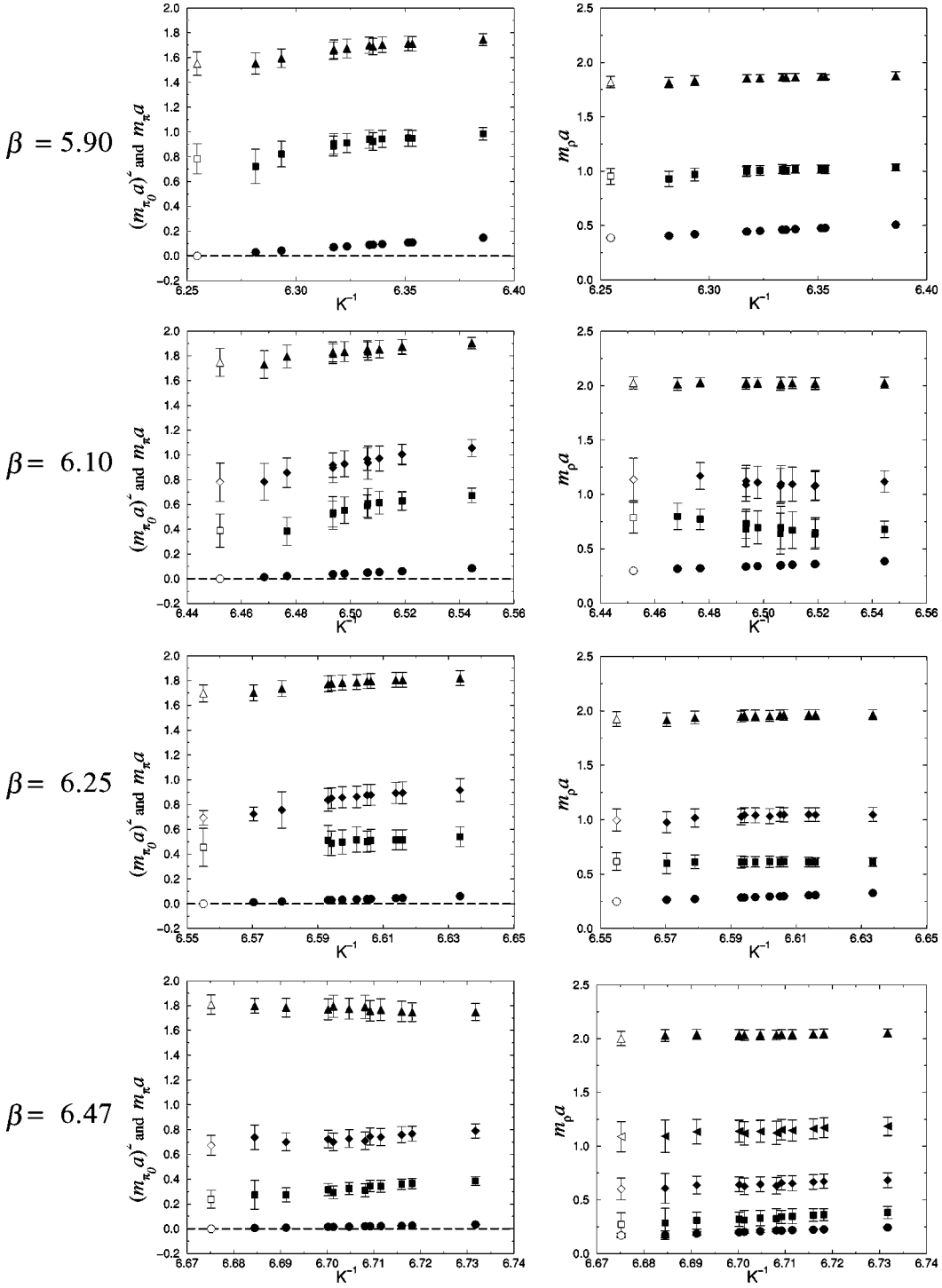

FIG. 7. Masses and their chiral extrapolations at all β. On the left hand side the π meson mass and on the right hand side the ρ meson mass are shown. Circles, squares, diamonds, and left triangles represent the ground, the first excited, the second excited, and the third excited state masses, respectively. The state shown by up triangles is considered unphysical as discussed in the text. Open symbols stand for the values in the chiral limit.

$$\langle 0|(\bar{d}\gamma_5 u)_{lat}|\pi_0,\mathbf{p}=\mathbf{0}\rangle = \frac{\sqrt{2}f_\pi m_\pi^2}{(m_u+m_d)^{AWI}_{lat}}\frac{1}{Z_A}\prod_{i=1}^{2}\sqrt{\frac{1}{1-3\kappa_i/4\kappa_c}}, \tag{25}$$

$$\langle 0|(\bar{d}\gamma_\mu u)_{lat}|\rho_0,\mathbf{p}=\mathbf{0}\rangle = \sqrt{2}f_\rho m_\rho^2 \epsilon_\mu \frac{1}{Z_V}\prod_{i=1}^{2}\sqrt{\frac{1}{2\kappa_i}}. \tag{26}$$

We employ the one-loop result with tadpole improvement for the renormalization factor Z_A [20] given by $Z_A=1$

TABLE IV. Results obtained from the MEM analysis at each β. Lattice spacings from the standard analysis [9,10] are also listed.

β	5.90	6.10	6.25	6.47
$a(\mathrm{GeV}^{-1})$	0.503(6)	0.387(6)	0.321(5)	0.220(25)
a^{-1} (GeV)	1.986(25)	2.583(40)	3.105(53)	4.52(51)
a^{-1} (GeV) [9,10]	1.934(16)	2.540(22)	3.071(34)	3.961(79)
κ_c	0.159881(13)	0.154985(12)	0.152556(9)	0.149809(7)
		π meson		
m_{π_1}/m_{ρ_0}	2.02(31)	1.30(44)	1.82(62)	1.40(45)
m_{π_2}/m_{ρ_0}		2.61(51)	2.79(23)	3.95(64)
$m_{\pi_{\mathrm{unphys}}}/m_{\rho_0}$	4.00(25)	5.86(38)	6.84(29)	10.6(1.2)
f_{π_0}/m_{ρ_0}	0.1157(21)	0.1148(26)	0.1099(28)	0.119(14)
$\Gamma_{\pi_0}/m_{\rho_0}$	0.036(16)	0.028(14)	0.029(21)	0.007(4)
		ρ meson		
m_{ρ_1}/m_{ρ_0}	2.46(19)	2.63(47)	2.48(32)	1.59(67)
m_{ρ_2}/m_{ρ_0}		3.81(65)	4.02(41)	3.53(71)
m_{ρ_3}/m_{ρ_0}				6.3(1.0)
$m_{\rho_{\mathrm{unphys}}}/m_{\rho_0}$	4.69(14)	6.79(21)	7.76(30)	11.7(1.3)
f_{ρ_0}	0.2037(20)	0.2088(25)	0.2015(32)	0.178(34)
f_{ρ_1}	0.1133(46)	0.076(34)	0.102(15)	0.120(40)
$\Gamma_{\rho_0}/m_{\rho_0}$	0.032(19)	0.014(7)	0.008(5)	0.022(15)

$-0.316\alpha_V(1/a)$, and the bare quark masses $(m_u+m_d)^{AWI}_{lat}$ derived from the axial ward identity [10]. For the vector meson decay constant, we use a nonperturbative value for Z_{V} [10].

Decay constants can be extracted from the correlation function as follows. For the pseudoscalar meson we have

$$\sum_{\mathbf{x}} \langle 0|\bar{d}\gamma_5 u(\tau,\mathbf{x})(\bar{d}\gamma_5 u)^\dagger(0,\mathbf{0})|0\rangle = \sum_n \langle 0|\bar{d}\gamma_5 u|\pi_n\rangle\langle\pi_n|(\bar{d}\gamma_5 u)^\dagger|0\rangle \frac{e^{-E_n\tau}}{2E_n} \quad (27)$$

$$\rightarrow |\langle\pi_0|\bar{d}\gamma_5 u|0\rangle|^2 \frac{e^{-m_{\pi_0}\tau}}{2m_{\pi_0}}, \quad \tau\rightarrow\infty, \quad (28)$$

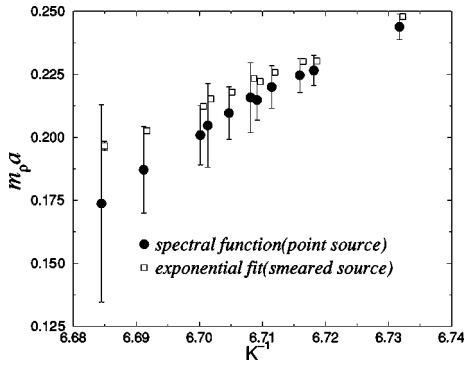

FIG. 8. Ground state masses of the ρ meson obtained by different analyses at $\beta=6.47$. Squares are slightly shifted to larger K^{-1}.

where E_n is the nth excited state energy, and a similar expression for the vector meson. Under the assumption that the ground state peak of the spectral function is sharp, these correlation functions are related to the area of the spectral function around the ground state peak according to

$$f_\pi^2=[(m_u+m_d)^{AWI}_{lat}]^2 \frac{\int_{peak} d\omega\, \rho_{\mathrm{PS}}(\omega)\omega^2}{m_\pi^3} Z_{\mathrm{A}}^2 \prod_{i=1}^{2}\left(1-\frac{3\kappa_i}{4\kappa_c}\right), \quad (29)$$

$$f_\rho^2=\frac{\int_{peak} d\omega\, \rho_{\mathrm{V}}(\omega)\omega^2}{m_\rho^3} Z_{\mathrm{V}}^2 \prod_{i=1}^{2} 2\kappa_i . \quad (30)$$

For the first excited state, we also extract decay constants from the area of the spectral function around the first excited state under the same assumption as for the ground state.

The decay constants obtained from the above relations are extrapolated linearly in K^{-1} to the chiral limit, as shown for $\beta=5.90$ in Fig. 10, and results are also given in Table IV. The decay constant for the first excited state of the π meson should vanish in the chiral limit according to Eq. (29); since the quark masses m_u+m_d vanish while the excited state mass m_{π_1} remains nonzero. This is in contrast to the ground state, for which the mass m_{π_0} vanishes in such a way that f_{π_0} remains nonzero. This property is seen in the figure.

The continuum extrapolation is shown in Fig. 11, and the results in the continuum limit are compiled in Table VI. For the ground state, the decay constants for π and ρ mesons are

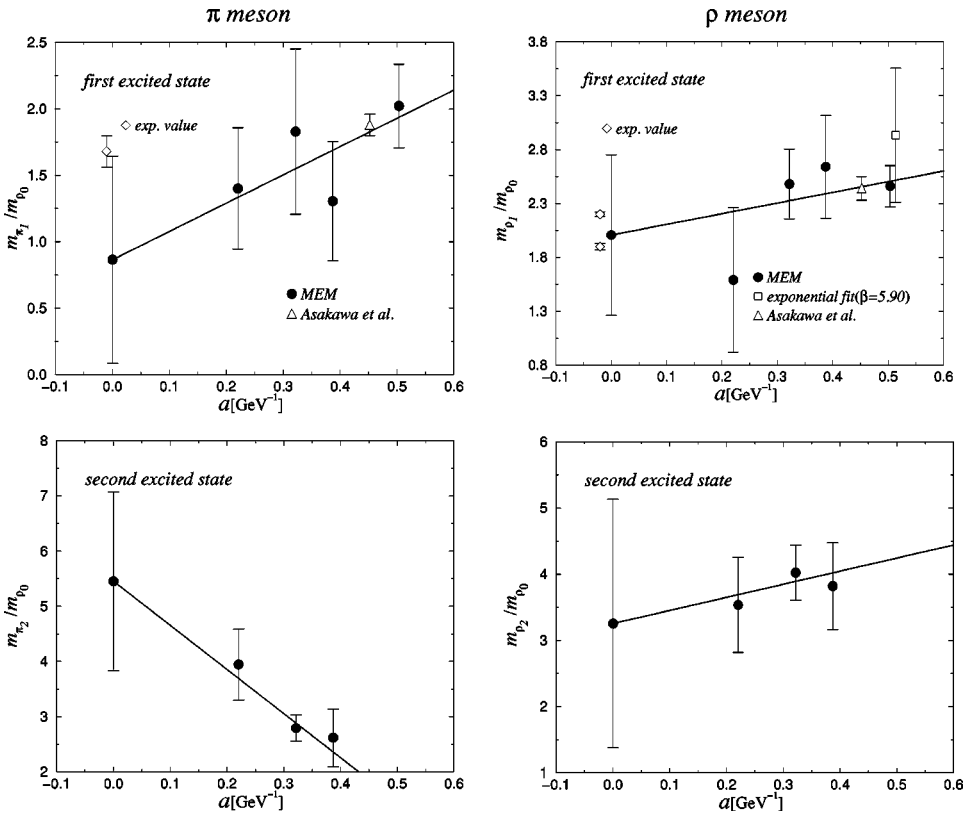

FIG. 9. Continuum extrapolation of masses of physical excited states. For the first excited state, open diamonds and triangles represent the experimental value, and that obtained by Asakawa *et al.* [5]. For the ρ meson the open square shows the result of the double exponential fit at $\beta=5.90$.

consistent with previous results (squares) [10]. In the continuum limit we find $f_{\pi_0}=80.3(5.9)$ MeV, which is smaller than the experimental value 93 MeV, and $f_{\rho_0}=0.2062(84)$, which is slightly larger than the experimental value 0.198(4), and the first excited state decay constant for the ρ meson $f_{\rho_1}=0.085(36)$.

D. Remark on spectral widths

The width for the ground state peak should be zero for the π meson, and should be very small for the ρ meson in the quenched approximation. Therefore the width for the ground state in spectral functions, if nonzero, is likely to be an artifact of the MEM. The widths Γ of the ground state peak for π and ρ mesons are extrapolated to the chiral limit, and are compiled in Table IV. As shown in Fig. 12, these widths are very small and almost consistent with zero within errors, as expected.

On the other hand, other states have larger widths. At this moment it is difficult to conclude whether these widths are physical or artifacts of the MEM. In order to decide the nature of these widths, further research is needed.

TABLE V. Masses of excited states normalized by the ground state ρ meson mass for the π and ρ mesons in the continuum limit. Available experimental values are also given. DOF indicates degrees of freedom.

	m_{π_1}/m_{ρ_0}	m_{π_2}/m_{ρ_0}	m_{ρ_1}/m_{ρ_0}	m_{ρ_2}/m_{ρ_0}
Continuum limit	0.86(77)	5.4(1.6)	2.00(74)	3.2(1.8)
χ^2/DOF	0.514	0.538	0.726	0.240
Experimental value	1.68(12)		1.90(3) or 2.20(2)	

V. UNPHYSICAL STATES AND FERMION DOUBLERS

As mentioned in the previous section, the state in the pseudoscalar channel at $\omega a\approx 1.7$ and the one in the vector channel at $\omega a\approx 2$ appear with a large width in the spectral functions at all β. A similar state has also been observed in the Wilson quark action at $\beta=6.0$ ($a^{-1}=2.2$ GeV) of the plaquette gauge action [6] and at $\beta=4.1$ ($a^{-1}=1.1$ GeV) of a tree-level Symanzik improved gauge action [7]. We consider this state to be unphysical since its mass diverges toward the continuum limit. In fact the mass of this state can be fitted by $C_1/a+C_2$ in Fig. 13 (see Table VII for numerical details), together with a linear continuum extrapolation for the physical excited state. We also see from this figure that no physical excited states appear in the spectral function if its mass is larger than that of the unphysical state. At first sight, the state at $\omega a\approx 1$ seems to be a candidate for another unphysical state. We think, however, that this state is physical, since the position of the peak moves as β varies, and moreover such a state was not observed at a different lattice spacing [7].

We argue that the unphysical state is a bound state of two fermion doublers of the Wilson quark action as follows. The pole mass of a free quark with Wilson parameter $r=1$ is given by

$$M(n)=\frac{1}{a}\log(1+ma+2n), \quad n=0,1,2,3, \tag{31}$$

where $n=0$ corresponds to the physical quark, and $n\neq 0$

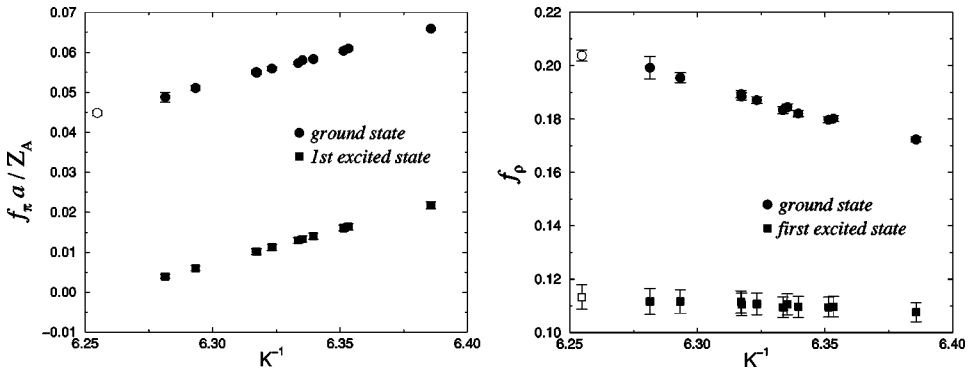

FIG. 10. Chiral extrapolations of pseudoscalar and vector meson decay constants at $\beta = 5.90$.

represent doublers with n of the three spatial momenta components equal to π/a. At $r=1$ the time doubler does not propagate due to its infinite mass. In the chiral limit the mass for the $n=1$ doubler is given by $M(1)a \approx 1.1$; therefore, in this free case, the mass of two $n=1$ doublers is $2 \times M(1)\, a \approx 2.2$. Note that, for meson correlation functions with zero spatial momentum, states consisting of, e.g., a physical quark and a doubler cannot contribute.

In the interacting case, the mass for the bound state made of two doublers is expected to decrease from 2.2 in the free theory due to the binding energy, which would depend on the quantum number of the state. This may explain the difference between the peak positions at $\omega a \approx 1.7$ for the pseudoscalar channel and at $\omega a \approx 2$ for the vector channel.

From the considerations above we conclude that the unphysical state is a bound state of two $n=1$ doublers. We note that bound states of $n \geqslant 2$ doublers do not appear in the spectral function [in fact there are no peaks at $\omega a = 3.2 \approx 2 \times M(2)\, a$ and $3.9 \approx 2 \times M(3)\, a$]. The reason for this is not understood at present. A possible explanation is that the state whose mass is close to the cutoff, π/a, is difficult to detect by the MEM, as seen in Fig. 5. Further work is needed, however, to clarify this point.

VI. CONCLUSION

In this study, we have applied the maximum entropy method to high-precision quenched lattice QCD data to extract the spectral functions for pseudoscalar and vector mesons. Masses for excited states as well as the ground state are obtained from the positions of peaks in the spectral function, and decay constants are determined from the area under them.

The masses of the ground and first excited states agree with those obtained by the usual double exponential fit with point and ground state smeared source data, showing the reliability of the MEM, while the first excited state mass from the spectral function has smaller errors, demonstrating the superiority of the MEM in this case.

We have been able to make a continuum extrapolation for

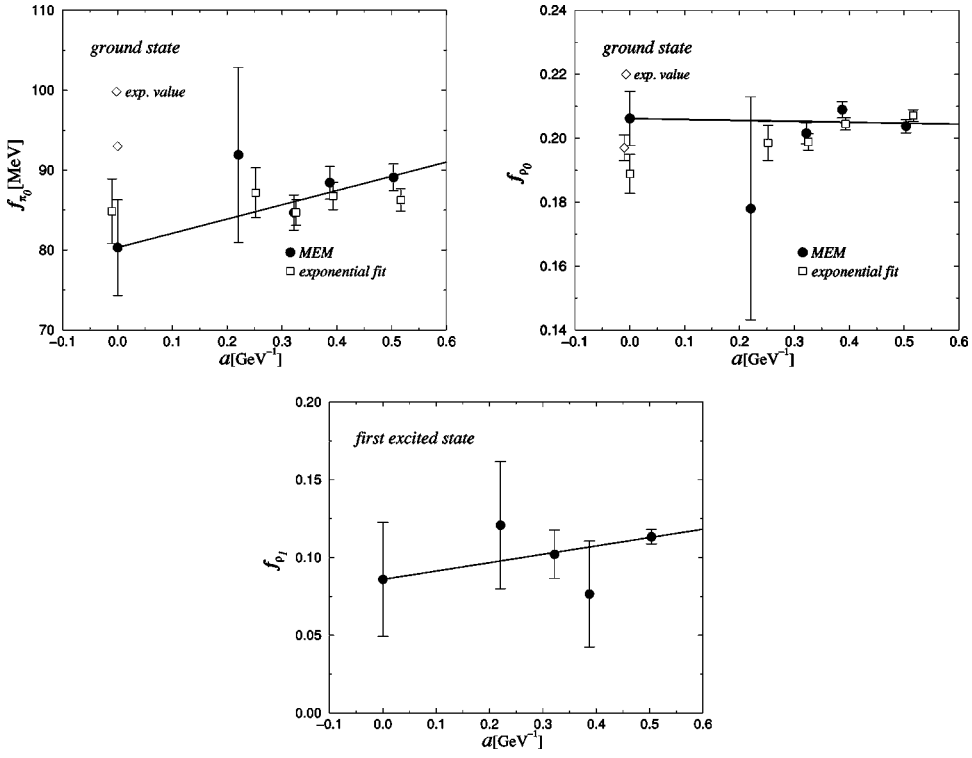

FIG. 11. Continuum extrapolations of pseudoscalar and vector meson decay constants. Open diamonds show experimental values for the ground state. Open squares represent the previous results from standard analysis [10].

TABLE VI. Decay constants for π and ρ mesons in the continuum limit and experimental values. DOF indicates degrees of freedom.

	f_{π_0}	f_{ρ_0}	f_{ρ_1}
Continuum limit	80.3(5.9) MeV	0.2062(84)	0.085(36)
χ^2/DOF	0.618	2.18	0.555
Experimental value	93 MeV	0.198(4)	

the first excited state for π and ρ mesons, obtaining the masses $m_{\pi_1}=660(590)$ MeV and $m_{\rho_1}=1540(570)$ MeV. While the errors are admittedly large, this is the first time that such an extrapolation has been attempted. For the ground state decay constant for π and ρ mesons we found that the result of the MEM analysis is consistent with standard analysis.

We have found a state in the meson spectral function at $\omega a \approx 2$ for all β, and have argued that it is an unphysical bound state of two fermion doublers. If this interpretation is correct, this will be the first time that the doubler state has been identified numerically in lattice QCD simulations. Further confirmation of this interpretation can be made by changing the Wilson parameter r from unity, by analyzing the Kogut-Susskind fermion data with the MEM, or by considering meson correlation functions with a momentum of π/a.

We have demonstrated that the masses and the decay constants for various states as well as the ground state spectral widths for both mesons can be extracted from a single correlation function with a point source by the MEM. While errors could be reduced by the standard analysis with more sophisticated methods, we think that the MEM can be a simple alternative.

A future extension of MEM analysis is an application to unquenched data to see dynamical quark effects in the spectral function; decays and scatterings of intermediate states may be detected from possible widths in the spectral function. It will also be interesting to see the change of the spectral function before and after the phase transition at finite temperatures.

ACKNOWLEDGMENTS

This work was supported in part by Grants-in-Aid of the Ministry of Education (Nos. 10640246, 10640248, 11640250, 11640294, 12014202, 12304011, 12640253, 12740133, and 13640260). The numerical calculations for the present work were carried out at the Center for Computational Physics, University of Tsukuba.

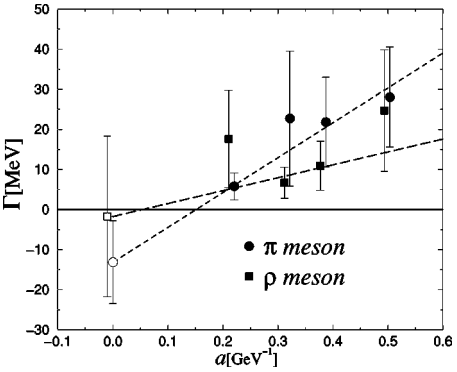

FIG. 12. Widths for the ground state peaks of π and ρ mesons and their continuum extrapolation.

APPENDIX A: BAYES'S THEOREM

In this section we list some results of probability theory and Bayes's theorem used in the MEM. Bayes's theorem in probability theory [11] is given by

$$\mathrm{P}[X|Y]=\frac{\mathrm{P}[Y|X]\,\mathrm{P}[X]}{\mathrm{P}[Y]}, \tag{A1}$$

where $\mathrm{P}[X]$ is the probability of an event X, and $\mathrm{P}[X|Y]$ is the conditional probability of X given Y. These probabilities satisfy

$$\mathrm{P}[X]=\int dY\,\mathrm{P}[X|Y]\,\mathrm{P}[Y], \tag{A2}$$

and the condition for normalization,

$$\int dX\,\mathrm{P}[X]=1, \tag{A3}$$

$$\int dX\mathrm{P}[X|Y]=1. \tag{A4}$$

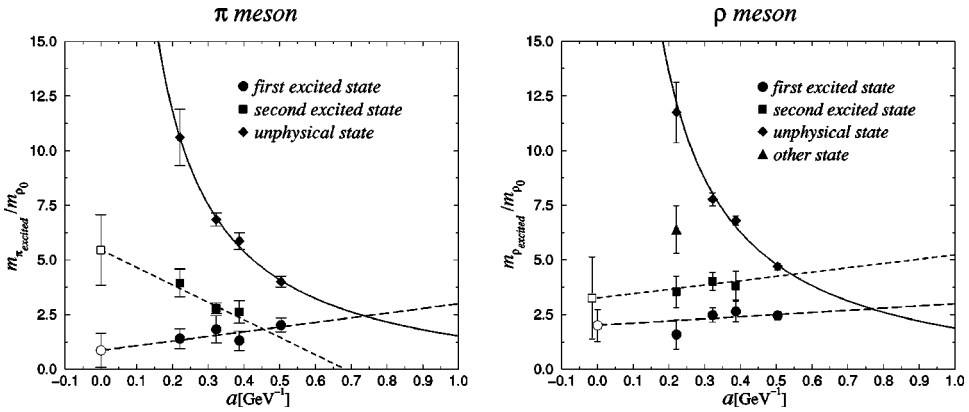

FIG. 13. Combination of the excited state mass fit and the unphysical state fit of π and ρ mesons.

TABLE VII. Fit parameters and χ^2/DOF (degrees of freedom) of the unphysical state fit for π and ρ mesons.

	π meson	ρ meson
C_1	2.57(30)	2.924(25)
C_2	−1.05(78)	−1.051(58)
χ^2/DOF	0.3158	1.476

In this article, we use $\mathrm{P}[X|YZ]$ which is the conditional probability of X given Y and Z. For $\mathrm{P}[X|YZ]$, Eqs. (A1), (A2), and (A4) are rewritten, respectively, as

$$\mathrm{P}[X|YZ]=\frac{\mathrm{P}[Y|XZ]\mathrm{P}[X|Z]}{\mathrm{P}[Y|Z]}, \tag{A5}$$

$$\mathrm{P}[X|Z]=\int dY\mathrm{P}[X|YZ]\mathrm{P}[Y|Z], \tag{A6}$$

$$\int dX\mathrm{P}[X|YZ]=1. \tag{A7}$$

The most probable spectral function is obtained by maximizing the conditional probability $\mathrm{P}[F|DH]$ (in this section prior knowledge $Hm\alpha$ is rewritten as H again for simplicity), and satisfies the condition,

$$\frac{\delta\mathrm{P}[F|DH]}{\delta F}=0. \tag{A8}$$

We rewrite $\mathrm{P}[F|DH]$ by Bayes's theorem as

$$\mathrm{P}[F|DH]=\frac{\mathrm{P}[D|FH]\mathrm{P}[F|H]}{\mathrm{P}[D|H]}. \tag{A9}$$

The probabilities $\mathrm{P}[D|FH]$ and $\mathrm{P}[F|H]$ are the likelihood function and the prior probability, respectively.

Integrating Eq. (A9) over F and using Eq. (A7), one finds that

$$\mathrm{P}[D|H]=\int \mathcal{D}F\mathrm{P}[D|FH]\mathrm{P}[F|H], \tag{A10}$$

where $\mathcal{D}F$ is the measure of the spectral functions. From this point of view, $\mathrm{P}[D|H]$ is a normalization factor related to the likelihood function and the prior probability, and we do not need to take account of it.

APPENDIX B: TRANSFORMATION OF COVARIANCE MATRIX

In this section we introduce a method that easily deals with a nondiagonal covariance matrix. If C is not a diagonal matrix, one can transform C into a diagonal form through $C=R\sigma^2R^{-1}$, where R is the transformation matrix and σ^2 is the eigenvalue matrix of C. The kernel $K_{li}=K(\omega_l,\tau_i)$ and the data $D_i=D(\tau_i)$ are transformed by R as

$$\tilde{K}_{li}=\sum_{i'=1}^{N_D} K_{li'}R_{i'i}, \tag{B1}$$

$$\tilde{D}_i=\sum_{i'=1}^{N_D} D_{i'}R_{i'i}. \tag{B2}$$

After this transformation, the likelihood function L defined in Eq. (6) is written as

$$L=\frac{1}{2}\sum_{i=1}^{N_D}\left(\tilde{D}_i-\sum_{l=1}^{N_\omega} f_l\tilde{K}_{li}\right)^2/\sigma_i^2. \tag{B3}$$

This transformation does not require any changes in other parts of the MEM.

APPENDIX C: THE NORMALIZATION CONSTANT OF THE PRIOR PROBABILITY

The factor $Z_S(\alpha)$ defined in Eq. (10) is the normalization constant of the prior probability. In order to calculate $Z_S(\alpha)$, we introduce a variable X_l that makes the curvature of $S(f)$ flat, and expand $S(f)$ by transforming f_l into X_l and applying the Gaussian approximation to $X(f)$ around $X(m)$,

$$\begin{aligned}S(f)\approx S(m)&+\sum_{l=1}^{N_\omega}\delta X_l\left.\frac{\partial S}{\partial X_l}\right|_{X(m)}\\&+\frac{1}{2}\sum_{l,l'=1}^{N_\omega}\delta X_l\delta X_{l'}\left.\frac{\partial^2 S}{\partial X_l\partial X_{l'}}\right|_{X(m)}\end{aligned} \tag{C1}$$

$$\begin{aligned}=S(m)&+\sum_{ll'}^{N_\omega}\delta X_l\left.\frac{\partial f_{l'}}{\partial X_l}\frac{\partial S}{\partial f_{l'}}\right|_m\\&+\frac{1}{2}\sum_{kk'll'}^{N_\omega}\delta X_l\delta X_{l'}\left.\frac{\partial f_k}{\partial X_l}\frac{\partial f_{k'}}{\partial X_{l'}}\frac{\partial^2 S}{\partial f_k\partial f_{k'}}\right|_m,\end{aligned} \tag{C2}$$

where $\delta X_l=X_l(f)-X_l(m)$. From the properties of X_l we choose

$$\frac{df_l}{dX_{l'}}=\sqrt{f_l}\delta_{ll'}. \tag{C3}$$

Since

$$S(m)=0,\quad \left.\frac{\partial S}{\partial f_l}\right|_m=0,\quad \left.\frac{\partial^2 S}{\partial f_l\partial f_{l'}}\right|_m=-\frac{1}{f_l}\delta_{ll'}, \tag{C4}$$

we take the Gaussian form for $S(f)$,

$$S(f)\approx-\frac{1}{2}\sum_{l=1}^{N_\omega}(\delta X_l)^2. \tag{C5}$$

The measure $\mathcal{D}F$ is derived from the so-called monkey argument [6,13,16] and related to the metric of $S(f)$. It is written as

$$\mathcal{D}F=\prod_{l=1}^{N_\omega}\frac{df_l}{\sqrt{f_l}}. \tag{C6}$$

$\mathcal{D}F$ is transformed by Eq. (C3) such that $\mathcal{D}F\to\Pi_{l=1}^{N_\omega}dX_l$. We can easily integrate over f_l and obtain the normalization constant,

$$Z_S(\alpha)=\int \mathcal{D}F e^{\alpha S(f)} \tag{C7}$$

$$\approx\int\prod_{l=1}^{N_\omega}dX_l\exp\left[-\frac{1}{2}\alpha\sum_{l}^{N_\omega}(\delta X_l)^2\right] \tag{C8}$$

$$=\left(\sqrt{\frac{2\pi}{\alpha}}\right)^{N_\omega}. \tag{C9}$$

APPENDIX D: UNIQUENESS OF THE MEM SOLUTION

In this section we explain that the condition satisfied by the most probable spectral function, Eq. (A8), has only one solution, and has no local minimum. The likelihood function L satisfies

$$\sum_{l,l'=1}^{N_\omega}z_l\frac{\partial^2(-L)}{\partial f_l\partial f_{l'}}z_{l'}=-\sum_{i=1}^{N_D}\frac{\tilde{z}_i^2}{\sigma_i^2}\leqslant 0\quad\text{with}\quad\tilde{z}_i=\sum_{l=1}^{N_\omega}z_lK_{li}, \tag{D1}$$

where the z_l's are nonzero real vectors and the $\tilde{z}_i$'s are real vectors. The entropy and a real and positive parameter α satisfy

$$\sum_{l,l'=1}^{N_\omega}z_l\frac{\partial^2\alpha S(f)}{\partial f_l\partial f_{l'}}z_{l'}=-\alpha\sum_{l=1}^{N_\omega}\frac{z_l^2}{f_l}<0, \tag{D2}$$

where we have used $0\leqslant f_l<\infty$ and $0<\alpha<\infty$. The matrix $\partial^2Q_\alpha(f)/\partial f_l\partial f_{l'}$ is negative definite,

$$\sum_{l,l'=1}^{N_\omega}z_l\frac{\partial^2Q_\alpha(f)}{\partial f_l\partial f_{l'}}z_{l'}<0. \tag{D3}$$

Using Rolle's theorem, one can verify that Eq. (A8) has only one solution corresponding to the global maximum of $Q_\alpha(f)$, if it exists [6]. Roughly speaking, since the curvature of $Q_\alpha(f)$ is always negative, $Q_\alpha(f)$ has only one maximum.

APPENDIX E: THE CALCULATION OF P[$\alpha|DHM$]

In order to search for the most probable value of α, we need to evaluate the conditional probability P[$\alpha|DHm$]. This conditional probability is used in Bryan's method [17] as the weight factor for averaging over α. In order to calculate P[$\alpha|DHm$], we transform P[$\alpha|DHm$] by Bayes's theorem and Eq. (A6) as

$$\mathrm{P}[\alpha|DHm]=\mathrm{P}[D|Hm\alpha]\mathrm{P}[\alpha|Hm]/\mathrm{P}[D|Hm] \tag{E1}$$

$$=\mathrm{P}[\alpha|Hm]\int\mathcal{D}F\,\mathrm{P}[D|FHm\alpha]\times\mathrm{P}[F|Hm\alpha]/\mathrm{P}[D|Hm] \tag{E2}$$

$$\propto\mathrm{P}[\alpha|Hm]\int\mathcal{D}F\frac{e^{Q_\alpha(f)}}{Z_LZ_S(\alpha)}. \tag{E3}$$

Under the assumption that P[$F|DHm\alpha$] is sharply peaked around the most probable spectral function f_α, $Q_\alpha(f)$ is expanded in the variable $X_l(f)$ used in Appendix C and the Gaussian approximation around $X_l(f)=X_l(f_\alpha)$,

$$Q_\alpha(f)\approx Q_\alpha(f_\alpha)+\sum_{l=1}^{N_\omega}\delta X_l\left.\frac{\partial Q_\alpha}{\partial X_l}\right|_{X(f_\alpha)}+\frac{1}{2}\sum_{l,l'=1}^{N_\omega}\delta X_l\delta X_{l'}\left.\frac{\partial^2Q_\alpha}{\partial X_l\partial X_{l'}}\right|_{X(f_\alpha)} \tag{E4}$$

$$=Q_\alpha(f_\alpha)+\sum_{ll'}^{N_\omega}\delta X_l\left.\frac{\partial f_{l'}}{\partial X_l}\frac{\partial Q_\alpha}{\partial f_{l'}}\right|_{f_\alpha}+\frac{1}{2}\sum_{kk'll'}^{N_\omega}\delta X_l\delta X_{l'}\left.\frac{\partial f_k}{\partial X_l}\frac{\partial f_{k'}}{\partial X_{l'}}\frac{\partial^2Q_\alpha}{\partial f_k\partial f_{k'}}\right|_{f_\alpha}, \tag{E5}$$

where $\delta X_l=X_l(f)-X_l(f_\alpha)$. Because

$$\left.\frac{\partial Q_\alpha}{\partial f_l}\right|_{f_\alpha}=0,\quad\left.\frac{\partial^2Q_\alpha}{\partial f_l\partial f_{l'}}\right|_{f_\alpha}=-\left(\frac{\alpha}{f_l}\delta_{ll'}+\frac{\partial^2L}{\partial f_l\partial f_{l'}}\right)_{f_\alpha}, \tag{E6}$$

we can write

$$Q_\alpha(f)\approx Q_\alpha(f_\alpha)-\frac{1}{2}\sum_{l,l'=1}^{N_\omega}\delta X_l(\alpha\delta_{ll'}+\Lambda_{ll'})\delta X_{l'}, \tag{E7}$$

where $\Lambda_{ll'}$ is a real symmetric $N_\omega\times N_\omega$ matrix defined as

$$\Lambda_{ll'}=\sqrt{f_l}\frac{\partial^2L}{\partial f_l\partial f_{l'}}\sqrt{f_{l'}}\Big|_{f_\alpha}. \tag{E8}$$

We then obtain

$$\mathrm{P}[\alpha|DHm]\approx\frac{\mathrm{P}[\alpha|Hm]}{Z_LZ_S(\alpha)}\int\prod_{l=1}^{N_\omega}dX_l\exp\left[Q_\alpha(f_\alpha)-\frac{1}{2}\sum_{l,l'}\delta X_l(\alpha\delta_{ll'}+\Lambda_{ll'})\delta X_{l'}\right] \tag{E9}$$

$$\propto\mathrm{P}[\alpha|Hm]\,e^{Q_\alpha(f_\alpha)}\prod_{l=1}^{N_\omega}\sqrt{\frac{\alpha}{\alpha+\lambda_l}}. \tag{E10}$$

Here the λ_l's are the eigenvalues of Λ.

APPENDIX F: ESTIMATION OF UNCERTAINTY IN THE MEM

In the MEM, it is possible to estimate the uncertainty of a spectral function averaged over a certain region I of ω,

$$\langle f_\alpha \rangle_{\mathrm{I}} = \frac{\int_{\mathrm{I}} d\omega \langle f(\omega) \rangle}{\int_{\mathrm{I}} d\omega} \approx \frac{\int_{\mathrm{I}} d\omega f_\alpha(\omega)}{\int_{\mathrm{I}} d\omega}, \tag{F1}$$

where $\langle \Theta \rangle = \int \mathcal{D}F \Theta \mathrm{P}[F|DHm\alpha]$. Using the Gaussian approximation and the variable $X_l(f)$ in Appendix E, the covariance of the spectral function can be calculated as

$$\langle \delta f(\omega) \delta f(\omega') \rangle = \sqrt{f_\alpha(\omega)} \langle \delta X(\omega) \delta X(\omega') \rangle \sqrt{f_\alpha(\omega')} \tag{F2}$$

$$\approx \sqrt{f_\alpha(\omega)} \Gamma^{-1}_{\omega\omega'} \sqrt{f_\alpha(\omega')} \tag{F3}$$

$$= -\left(\frac{\delta^2 Q_\alpha}{\delta f(\omega) \delta f(\omega')} \right)^{-1}_{f_\alpha}, \tag{F4}$$

where $\Gamma = \alpha\delta + \Lambda$. The form of Eq. (F4) is readily available because it is the Hessian of the Newton search algorithm [3,6,17] used to find f_α. The uncertainty is estimated as

$$\langle (\delta f_\alpha)^2 \rangle_{\mathrm{I}} \approx \frac{\int_{\mathrm{I}\times\mathrm{I}} d\omega d\omega' \sqrt{f_\alpha(\omega)} \Gamma^{-1}_{\omega\omega'} \sqrt{f_\alpha(\omega')}}{\int_{\mathrm{I}\times\mathrm{I}} d\omega d\omega'}. \tag{F5}$$

Similar to the spectral function, the error of the averaged spectral function in a certain region I is averaged over α with the weight factor $\mathrm{P}[\alpha|DHm]$,

$$\langle \delta \hat{f} \rangle_{\mathrm{I}} = \frac{\int d\alpha \mathrm{P}[\alpha|DHm] \sqrt{\langle (\delta f_\alpha)^2 \rangle_{\mathrm{I}}}}{\int d\alpha \mathrm{P}[\alpha|DHm]}. \tag{F6}$$

[1] L. Maiani and M. Testa, Phys. Lett. B **245**, 585 (1990).
[2] L. Lellouch and M. Lüscher, Commun. Math. Phys. **219**, 31 (2001).
[3] M. Jarrell and J.E. Gubernatis, Phys. Rep. **269**, 133 (1996).
[4] Ph. de Forcrand *et al.*, Nucl. Phys. B (Proc. Suppl.) **63**, 460 (1998).
[5] Y. Nakahara, M. Asakawa, and T. Hatsuda, Phys. Rev. D **60**, 091503 (1999).
[6] M. Asakawa, T. Hatsuda, and Y. Nakahara, Prog. Part. Nucl. Phys. **46**, 459 (2001).
[7] I. Wetzorke and F. Karsch, presented at International Workshop on Strong and Electroweak Matter (SEWM 2000), hep-lat/0008008.
[8] M. Oevers, C. Davies, and J. Shigemitsu, Nucl. Phys. B (Proc. Suppl.) **94**, 423 (2001); hep-lat/0009031.
[9] CP-PACS Collaboration, S. Aoki *et al.*, Phys. Rev. Lett. **84**, 238 (2000).
[10] CP-PACS Collaboration, S. Aoki *et al.* (unpublished).
[11] A. Papoulis, *Probability and Statistics* (Prentice-Hall, New York, 1990), p. 422.
[12] S. Brandt, *Statistical and Computational Methods in Data Analysis* (North-Holland, Amsterdam, 1983).
[13] J. Skilling, in *Maximum Entropy and Bayesian Methods*, edited by J. Skilling (Kluwer Academic, Dordrecht, 1989), p. 45.
[14] S. F. Gull, in *Maximum Entropy and Bayesian Methods* (Ref. [13]), p. 53.
[15] J. Skilling, in *Maximum Entropy and Bayesian Methods in Science and Engineering*, edited by G. J. Erickson and C. R. Smith (Kluwer Academic, Dordrecht, 1988), p. 173.
[16] E. T. Jaynes, in *Maximum Entropy and Bayesian Methods in Applied Statistics*, edited by J. H. Justice (Cambridge University Press, Cambridge, England, 1986), p. 26.
[17] R. K. Bryan, Eur. Biophys. J. **18**, 165 (1990).
[18] E. V. Shuryak, Rev. Mod. Phys. **65**, 1 (1993).
[19] L. J. Reinders, H. Rubinstein, and S. Yazaki, Phys. Rep. **127**, 1 (1985).
[20] G. P. Lepage and P. B. Mackenzie, Phys. Rev. D **48**, 2250 (1993); G. P. Lepage, Nucl. Phys. B (Proc. Suppl.) **26**, 45 (1992); A. S. Kronfeld, *ibid.* **30**, 445 (1993); P. B. Mackenzie, *ibid.* **30**, 35 (1993).